

Dual-branch Robust Unlearnable Examples

Xianlong Wang¹ Hangtao Zhang² Wenbo Pan¹ Ziqi Zhou² Changsong Jiang³ Li Zeng⁴ Xiaohua Jia¹

Abstract

Unlearnable examples (UEs) aim to compromise model training by injecting imperceptible perturbations to clean samples. However, existing UE schemes exhibit limited robustness against advanced defenses due to their heuristic design or narrowly scoped domain perturbations. To address this, we propose DUNE, a **D**ual-branch **U**nlearnable **E**nsemble perturbation optimization approach. Specifically, DUNE separately optimizes perturbations in the spatial and color domains to establish the mapping between perturbations and shift-induced labels. This design extends the perturbation domain to increase noise intensity for improving robustness and drives the models to learn perturbation-oriented features with degraded generalization, thereby achieving unlearnability. To strengthen DUNE’s performance, we further propose an unlearnability-enhancing ensemble strategy that aggregates diverse pre-trained models during the dual-branch optimization. Extensive experiments on benchmark datasets CIFAR-10 and ImageNet verify that DUNE’s robustness outperforms 12 SOTA UE schemes under 7 mainstream defenses, yielding a lower average test accuracy of 14.95% to 50.82%. The code is available at <https://github.com/wxldragon/DUNE>.

1. Introduction

With the flourishing development of *deep neural networks* (DNNs), a large number of machine learning platforms obtain public training data through web crawling (Carlini et al., 2024; Baack, 2024). Given this, *unlearnable examples* (UEs) (Huang et al., 2021; Wang et al., 2024b; Yu

¹Department of Computer Science, City University of Hong Kong, Hong Kong SAR, China ²Huazhong University of Science and Technology, Wuhan, China ³University of Electronic Science and Technology of China, Chengdu, China ⁴Changsha University of Science and Technology, Changsha, China.

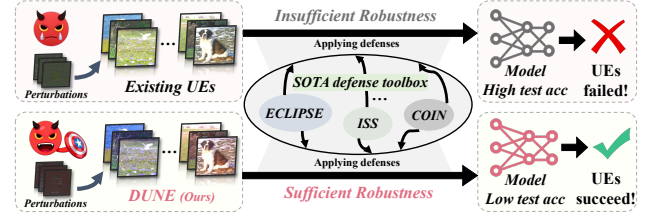


Figure 1. **Overview of UEs.** Existing UE schemes fail to compromise DNNs due to insufficient robustness, whereas our proposed scheme DUNE remains robust under these SOTA defenses.

et al., 2025; Sun et al., 2024; Wu et al., 2025) are proposed to make data "unlearnable" for deep learning models via adding imperceptible perturbations to clean images, thereby compromising model performance.

At a high level, UEs (Wu et al., 2023; Huang et al., 2021; Yu et al., 2022) exploit the tendency of DNNs to favor learning simpler shortcut (Geirhos et al., 2020; Wang et al., 2024c) features, establishing a mapping between perturbation features and labels for achieving unlearnability. To this end, existing UE schemes (Huang et al., 2021; Sandoval-Segura et al., 2022; Wu et al., 2023; Liu et al., 2024a; Sadasivan et al., 2023) typically search for *shortcut perturbations* easily captured by DNNs while ensuring perturbation stealthiness. However, such strategies primarily suffer from two limitations: (i) *Heuristic shortcut pattern*. Certain UEs (Yu et al., 2022; Sadasivan et al., 2023) tend to adopt empirical shortcut patterns directly as perturbations without formal optimization, rendering them easily compromised by adaptive defenses (Li et al., 2025; Liu et al., 2023); (ii) *Domain-constrained perturbation optimization*. Existing UE methods (Fu et al., 2022; Chen et al., 2023; Meng et al., 2024) further optimize perturbations to achieve unlearnability, using a single-domain constraint for preserving visual quality, which results in homogeneous perturbations vulnerable to noise-suppressing defenses (Wang et al., 2024a; Liu et al., 2023). Therefore, existing UE approaches exhibit insufficient robustness when confronted with the *state-of-the-art* (SOTA) defense toolbox, as demonstrated in Fig. 1. This motivates us to raise an intriguing research question:

Is it possible to optimize shortcut perturbations across diverse domains while ensuring robustness?

In response, we propose a **D**ual-branch **U**nlearnable **E**nsemble scheme (DUNE) that optimizes perturbations

in both the spatial and color domains for establishing a perturbation-to-label mapping. The orthogonality between these domains enriches perturbation diversity and thereby enhances robustness against various defenses. Specifically, we optimize perturbations in the feature space toward shift-induced labels that are displaced from the true labels, thereby forming a mapping from perturbations to shifted labels and achieving unlearnability. Following this principle, we decompose the joint dual-domain optimization into two independent sub-optimization problems, each optimizing perturbations within its respective domain. For spatial branch generation, we drive ℓ_∞ -norm perturbations so that their features approach the shift-induced labels according to each sample’s category, where the ℓ_∞ constraint guarantees perturbation stealthiness and the perturbation is optimized via T -step *project gradient descent* (PGD) (Madry et al., 2018). For color branch generation, our insight is to increase the orthogonality between color and spatial perturbations so as to reduce the overlap of shortcut patterns, thereby increasing perturbation diversity for improved robustness. To this end, the color perturbations are generated via shifting luminance corresponding to the *direct current* (DC) component, which is independent of the spatial perturbations in the *alternating current* (AC) components. In particular, distinct luminance-shifted unlearnable offsets are injected into each RGB channel, and a class-wise strategy with the gradient-free *particle swarm optimization* (PSO) (Wang et al., 2018) is employed to align them with the shift-induced labels. Finally, to further enhance DUNE’s unlearnability and robustness, we adopt the concept of ensemble learning (Dong et al., 2020), merging gradient or loss from a pre-trained model gallery during optimization to enrich the spectrum of perturbations, thus enhancing robustness.

Extensive experiments on benchmark datasets CIFAR-10 (Krizhevsky & Hinton, 2009) and ImageNet (Deng et al., 2009) verify that our proposed DUNE achieves superior robustness against 12 SOTA UE schemes under 7 strong defenses, accompanied by a lower average test accuracy of 14.95%~50.82% on CIFAR-10. Beyond this, to evaluate DUNE under more challenging scenarios, we design two adaptive defenses (*i.e.*, assuming awareness of spatial-color domain knowledge) against DUNE, with experimental results on four diverse models confirming its robustness. Our main contributions are summarized as:

- ◆ We propose DUNE, a dual-domain unlearnable optimization scheme that generates spatial and color perturbations to align features with shift-induced labels, exhibiting sufficient robustness against defenses.
- ◆ We propose an unlearnability-enhancing ensemble module that aggregates gradient information from a model gallery to enhance effectiveness and robustness.
- ◆ We conduct extensive experiments on multiple bench-

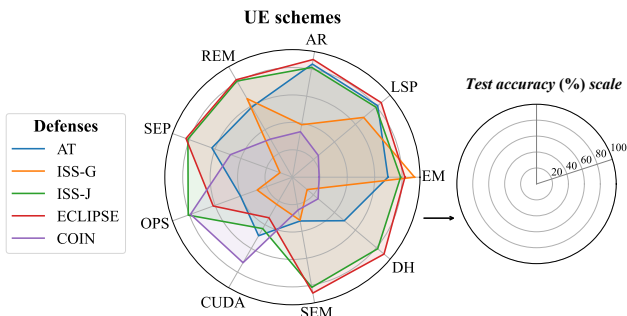


Figure 2. **Quantitative UE robustness** (in test accuracy, %) under five defenses with CIFAR-10 (Krizhevsky & Hinton, 2009) trained on ResNet18 (He et al., 2016). A point’s proximity to the outer boundary signifies lower UE robustness, highlighting the limited robustness in existing UE schemes.

mark datasets and models, demonstrating that DUNE achieves superior robustness over 12 SOTA UE approaches under both existing and adaptive defenses.

2. Related Work

2.1. Unlearnable Examples

Unlearnable examples (UEs) introduce imperceptible perturbations to training samples, thereby degrading the generalization performance of unauthorized models. Existing UE schemes primarily generate perturbations under ℓ_p -norm constraints in the spatial domain, such as ℓ_∞ methods *error-minimization* (EM) (Huang et al., 2021), *self-ensemble perturbation* (SEP) (Chen et al., 2023), and *stable error-minimization* (SEM) (Liu et al., 2024b), ℓ_2 approaches *linearly separable perturbation* (LSP) (Yu et al., 2022) and *autoregressive perturbation* (AR) (Sandoval-Segura et al., 2022), and the ℓ_0 scheme *one-pixel shortcut* (OPS) (Wu et al., 2023). Although these UEs achieve considerable unlearnability, their perturbations are constrained within an ℓ_p -norm ball in the single spatial domain, rendering them vulnerable to noise-suppression defenses (Liu et al., 2023; Wang et al., 2024a; Tao et al., 2021) and thus lacking robustness. Another branch of UEs involves heuristic perturbation design, *e.g.*, convolutional noise CUDA (Sadasivan et al., 2023), which lacks of robustness under the adaptive defense (Li et al., 2025). Thus, existing studies highlight the need for a more robust UE scheme.

2.2. Defenses Against UEs

Tao et al. (Tao et al., 2021) first employ *adversarial training* (AT) (Madry et al., 2018) defense to break unlearnability, but it is afterwards defeated by the *robust error-minimization* (REM) (Fu et al., 2022) UE scheme trained with adversarial perturbations. Subsequently, *orthogonal projection-based* (OP) (Sandoval-Segura et al., 2023) and VAE-based (Yu et al., 2024a) approaches are proposed, enriching the defensive landscape. Beyond these defense methods, mainstream

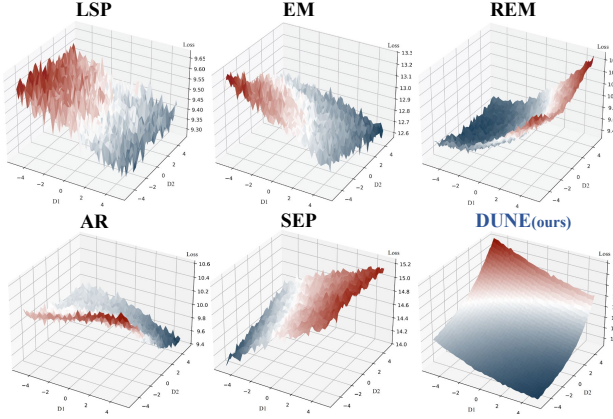


Figure 3. Visualization of loss landscapes for ResNet18 trained on five single-domain UEs (LSP (Yu et al., 2022), EM (Huang et al., 2021), REM (Fu et al., 2022), AR (Sandoval-Segura et al., 2022), SEP (Chen et al., 2023)) and our DUNE on CIFAR-10.

defenses include diffusion purification approaches (Wang et al., 2024a; Dolatabadi et al., 2023; Jiang et al., 2023) such as ECLIPSE (Wang et al., 2024a) and *image shortcut squeezing* (ISS) defense such as ISS-J (Liu et al., 2023), both of which can defeat existing single-domain UEs. Additionally, an adaptive defense COIN (Li et al., 2025) that employs random matrix transformation addresses convolutional UEs, further revealing the insufficient robustness of existing UEs, as quantitatively illustrated in Fig. 2.

3. Preliminaries

3.1. Problem Formulation

UE’s goal. As data publishers intend to prevent the data from being exploited to train unauthorized DNNs \mathcal{F} , they integrate imperceptible noise δ_u to clean training samples $x \in \mathbb{R}^{C \times H \times W}$ to form the *unlearnable examples* (Huang et al., 2021; Fu et al., 2022; Zhu et al., 2024; Yu et al., 2024b), resulting in low generalization performance. Formally, the goal of UEs is to satisfy the following objectives:

$$\max_{(x', y') \sim \mathcal{D}_t} \mathbb{E} \mathcal{L}(\mathcal{F}(x'; \theta^*), y'), \quad (1)$$

$$\text{s.t. } \theta^* = \arg \min_{\theta} \sum_{(x, y) \in \mathcal{D}_c} \mathcal{L}(\mathcal{F}(x + \delta_u; \theta), y) \quad (2)$$

where δ_u refers to the perturbation applied to x to serve as the unlearnable example $x_u = x + \delta_u$, y denotes the ground-truth label, (x', y') refers to data sampled from the clean testing distribution \mathcal{D}_t , \mathcal{D}_c is clean training set, \mathcal{L} represents the loss function, e.g., cross-entropy loss, and θ^* denotes the optimized model parameters.

Existing UE studies generate δ_u within a single domain, typically the spatial domain Φ_s instantiated by an ℓ_p -norm ball space, i.e., $\|\delta_u\|_p \leq \epsilon$. Such single-domain perturbations are easily compromised by existing defenses (Wang et al.,

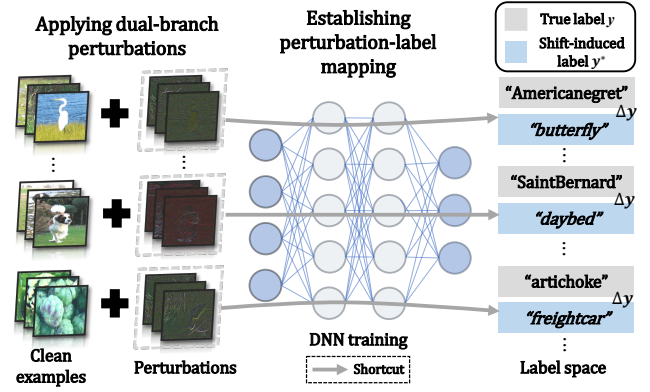


Figure 4. An intuitive understanding of DUNE’s objective that pushes features toward the shift-induced class in a class-wise way.

2024a), leading to the minimization of Eq. (1)’s expectation term, i.e., UEs lack robustness against defenses.

A typical UE design. Beyond achieving UE objectives in Eqs. (1) and (2), several studies (Fu et al., 2022; Sadasivan et al., 2023; Meng et al., 2024) also increase the robustness of UEs against defenses, among which we select REM (Fu et al., 2022) as a representative. REM aims to minimize the adversarial loss by solving a min-min-max tri-level optimization problem to generate UEs, thereby enhancing robustness against AT (Tao et al., 2021). Specifically, the objective of generating perturbations is formulated as follow:

$$\min_{\delta_u} \mathbb{E}_{(x, y) \sim \mathcal{D}_c} \left[\min_{\|\delta_u\|_\infty \leq \epsilon_u} \max_{\|\delta_a\|_\infty \leq \epsilon_a} \mathcal{L}(f_\theta^*(x + \delta_u + \delta_a), y) \right] \quad (3)$$

where δ_u denotes the unlearnable noise constrained within the norm range of ϵ_u , and δ_a represents the ϵ_a -bounded adversarial noise, f_θ^* denotes a randomly initialized network. REM optimizes Eq. (3) to drive $x_u = x + \delta_u$ toward class y in feature space, thereby achieving unlearnability. Despite REM’s robustness to AT due to tri-level optimization, restricting δ_u to a single ℓ_∞ domain confines the perturbation range, leaving it susceptible to stronger defenses (Wang et al., 2024a; Liu et al., 2023), as shown in Fig. 2.

3.2. Limitations of Existing Efforts

As previously discussed, existing UE schemes (Fu et al., 2022; Liu et al., 2024b; Meng et al., 2024; Wu et al., 2023) exhibit insufficient robustness against powerful defenses (Wang et al., 2024a; Liu et al., 2023), and this limitation can be attributed to two key factors: **1 Heuristic shortcut design.** Some existing UE approaches overly rely on empirically designed simple shortcut patterns, such as linear block perturbations (Yu et al., 2022) or convolutional noise (Sadasivan et al., 2023), without a principled optimization formulation. Such perturbations can be easily exploited by adaptive defenses (Li et al., 2025; Liu et al., 2023) to fully capture internal mechanisms and defeat them; **2 Domain-limited perturbation generation.** Existing UE

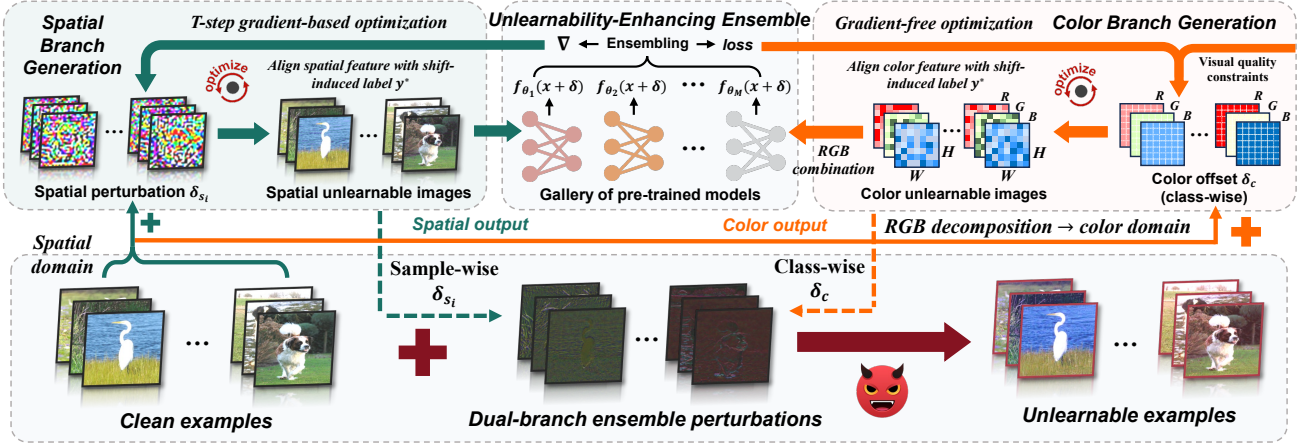


Figure 5. The framework of DUNE.

schemes (Huang et al., 2021; Fu et al., 2022; Chen et al., 2023) optimize perturbations within a single domain, which confines them to a limited feature space and causes non-smooth and locally oscillating structures as shown in Fig. 3. Such loss landscapes rely on a single frequency pattern and are thereby fragile against defenses like ISS-J (Liu et al., 2023), which suppress frequency information. By comparison, DUNE yields a smoother landscape, highlighting the robustness of perturbations (Pham et al., 2024).

4. Methodology

4.1. Design Principle

To address the limitations of existing UEs, our design principles are listed as follows: **1 Feature misalignment optimization.** Given the fragility of heuristic designs, our principle is to increase the complexity of shortcut perturbations by minimizing the distance between features and shift-induced classes. Specifically, for each class, samples are optimized to approach the class shifted by the same label offset, as illustrated in Fig. 4. In this way, DNNs establish a mapping between perturbations and shift-induced labels, preventing them from learning sample features and reducing generalization ability; **2 Dual-branch perturbation design.** UEs (Wu et al., 2023) typically exploit shortcut perturbations (Geirhos et al., 2020) that contain simple features for DNN learning (similar to backdoors (Hu et al., 2023; Zhang et al., 2024; Wang et al., 2024d)). Therefore, such shortcut noise may reside in any domain of image data, provided it remains easily learned by DNNs. Meanwhile, as complementary to the spatial domain, the color domain (Zhao et al., 2023; Wang et al., 2022) yields color perturbations that follow a fundamentally different distribution from the Gaussian noise purified in ECLIPSE (Wang et al., 2024a), while its low-frequency nature enhances resilience to high-frequency compression defense ISS-J (Liu et al., 2023). Given these insights, our principle is to optimize perturbations in dual

domains to increase noise diversity, thus boosting UE robustness.

4.2. A High-level Objective

Pushing perturbations closer to shift-induced class. Our idea is to generate shortcut perturbations in both the spatial domain Φ_s and the color domain Φ_c for establishing the mapping between dual-domain perturbation features and labels. Specifically, the perturbations are optimized toward the shift-induced classes y^* in feature space, establishing a class-wise offset mapping as shown in Fig. 4. In this way, owing to their tendency to rely on shortcuts rather than intrinsic sample features, DNNs suffer from poor generalization, *i.e.*, satisfying Eqs. (1) and (2), while perturbing across domains strengthens UE robustness. Formally, the high-level objective of DUNE is defined as:

$$\min_{\delta_u} \mathbb{E}_{(x,y) \sim \mathcal{D}_c} [\mathcal{L}_{\text{CE}}(f_{\theta}(\psi(x; \delta_u)), y^*)], \quad (4)$$

$$\text{s.t. } \delta_u \in \Phi_s \times \Phi_c, \quad y^* = (y + \Delta y) \bmod k \quad (5)$$

where perturbation δ_u is derived in spatial-color domain, f_{θ} is a pre-trained network, \mathcal{L}_{CE} is cross-entropy loss, ψ denotes the operation of applying δ_u to sample x to generate the UE, y is the true label, Δy indicates the label deviation (see Fig. 4), and k refers to the number of categories in \mathcal{D}_c .

Grounded in the spatial-color perturbations, we analyze the robustness as presented below:

Remark I (Frequency perspective)

Spatial unlearnable perturbations concentrate on high-frequency components, enabling them to bypass low-frequency defenses such as ISS-G; color unlearnable perturbations reside in low-frequency components, allowing them to evade defenses, e.g., ECLIPSE and ISS-J, thus yielding broader and superior robustness due to orthogonal design.

4.3. A Ground-level Design: DUNE

Unlearnable domain decomposition. To reduce the complexity of dual-domain unlearnable objective in Eqs. (4) and (5), our key intuition is that both *independent* and *joint* dual-branch optimization exert negligible influence on the shift-induced mapping. From this perspective, we simplify the original joint optimization problem into two distinct domain-wise optimization problems (*i.e.*, $\delta_u \triangleq \delta_s \oplus \delta_c$) via decomposing the objective, each solved independently and re-formulated as follows:

$$\min_{\delta_d \in \Phi_d} \mathbb{E}_{(x,y) \sim \mathcal{D}_c} [\mathcal{L}_{\text{CE}}(f_\theta(\psi(x; \delta_d)), y^*)], d \in \{s, c\} \quad (6)$$

$$x_u = \psi(x; \delta_c, \delta_s) \quad (7)$$

where (δ_d, Φ_d) corresponds to two domain-specific cases, each optimized separately by using Eq. (6) to obtain spatial perturbation δ_s and color perturbation δ_c , which are then integrated through ψ to produce x_u .

Spatial branch optimization. For spatial-domain unlearnable realization, we instantiate Φ_s as a domain formed by an ℓ_∞ -norm ball sphere, formally expressed as: $\|\delta_s\|_\infty \leq \epsilon$, where ϵ is the norm constraint. Nevertheless, Eq. (6) for the spatial branch remains an intractable non-convex optimization. Given the perturbation is optimized in a class-wise deviation manner, we employ the T -step *project gradient descent* (PGD) (Madry et al., 2018) on the shift-induced label-based loss ranging from the classes. Assuming the clean dataset \mathcal{D}_c is formulated as:

$$\mathcal{D}_c = \left\{ \underbrace{(x_1, y_p), (x_2, y_p), \dots, (x_{n_p}, y_p)}_{n_p \text{ samples from class } y_p} \right\}_{p=1}^k \quad (8)$$

where k is the number of classes. For each sample $x_i \in \{x_i\}_{i=1}^{n_p}$ belonging to ground-truth label y_p , we derive the perturbation δ_{s_i} in the spatial domain to align its feature with shift-induced class y_p^* as follows:

$$g_t = \nabla_{x_i^t} \mathcal{L}_{\text{CE}}(f_\theta(x_i^t), y_p^*), \quad y_p^* = (y_p + \Delta y) \bmod k \quad (9)$$

$$x_i^{t+1} = x_i^t - \beta \cdot \text{sign}(g_t) \Big|_{t=0}^{T-1} \quad (10)$$

$$x_i^{t+1} = \min \left\{ \max \{ x_i^{t+1}, x_i^0 - \epsilon \}, x_i^0 + \epsilon \right\} \Big|_{t=0}^{T-1} \quad (11)$$

where $x_i^0 = x_i$, $\delta_{s_i} = x_i^T - x_i^0$, g_t denotes the gradient at the t -th iteration, serving to optimize the spatial perturbation δ_{s_i} , β is the step size, and T is the number of iteration, after which the spatial branch generates spatial perturbation δ_{s_i} . Eq. (11) ensures that δ_{s_i} is produced within the ϵ -norm constraint, thus safeguarding sample visual quality.

Color branch optimization. *Motivation for luminance-shift perturbations.* An image can be decomposed into a *direct current* (DC) component representing block-wise mean

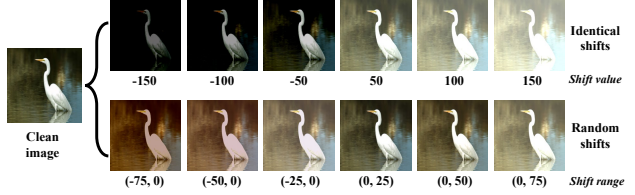


Figure 6. The luminance adjustment effect of applying identical pixel shifts and random pixel shifts to R , G , and B channels.

luminance and *alternating current* (AC) components where spatial perturbations concentrate their energy (Guo et al., 2025). Therefore, to promote orthogonality between dual-domain perturbations for enhancing robustness, the color branch aims to optimize perturbations for altering luminance targeting the DC component. As shown in Fig. 6, applying either identical or distinct random shifts to RGB channels alters luminance, where the identical pattern includes only a single tunable parameter, restricting the optimization flexibility. Hence, we apply distinct shifts to each RGB channel, increasing the perturbation dimensionality. Formally, we define this process applied to x_i as described below:

$$x_i \in \mathbb{R}^{3 \times H \times W} \xrightarrow{\text{decompose}} x_r, x_g, x_b \in \mathbb{R}^{1 \times H \times W}, \quad (12)$$

$$x_{u_i}^c = (x_r + \Delta x_r, x_g + \Delta x_g, x_b + \Delta x_b) \quad (13)$$

where Δx_r , Δx_g , and Δx_b denote the luminance-shifted unlearnable offsets applied to the RGB decomposition x_r , x_g , and x_b , $x_{u_i}^c$ is the color-branch UE, and the perturbation $\delta_{c_i} = x_{u_i}^c - x_i$. For establishing the mapping between color-branch features and shift-induced labels, we assign class-wise perturbation δ_{c_i} to samples based on categories.

Class-wise color-branch perturbation optimization. As the optimization in Eqs. (6) and (13) for δ_{c_i} does not rely on gradients, we adopt the gradient-free *particle swarm optimization* (PSO) (Wang et al., 2018) that employs particles to navigate color space Φ_c to converge toward perturbation δ_{c_i} with a class-wise mode. Additionally, as shown in Fig. 6, similarity functions PSNR (Tanchenko, 2014), SSIM (Bakurov et al., 2022), and LPIPS (Kettunen et al., 2019; Wang et al., 2026) are employed to constrain the color domain Φ_c . In light of these, from each class, we randomly select N samples $\{x_i\}_{i=1}^N$ to construct their loss objective for PSO-driven minimization as follows:

$$\min_{\delta_{c_i}} \mathbb{E}_{\{(x_i, y_p)\}_{i=1}^N} \left[\underbrace{\mathcal{L}_{\text{CE}}(f_\theta(x_i + \delta_{c_i}), y_p^*)}_{\text{unlearnability}} + \lambda \underbrace{\mathcal{L}_{nc}(x_i, x_i + \delta_{c_i})}_{\text{noise constraint}} \right], \quad (14)$$

$$\text{s.t.}, \quad \delta_{c_1} = \delta_{c_2} = \dots = \delta_{c_N} \equiv \delta_c \quad (15)$$

where δ_c denotes the same perturbation applied to samples $\{x_i\}_{i=1}^{n_p}$ from the same class y_p , whereas different classes employ different ones (*i.e.*, class-wise pattern), $\mathcal{L}_{nc} = \max(0, \tau_1 - \mathcal{L}_{\text{psnr}}) + \max(0, \tau_2 - \mathcal{L}_{\text{ssim}}) + \max(0, \mathcal{L}_{\text{lpiips}} - \tau_3)$, and $\tau_1, \tau_2, \tau_3, \lambda$ are pre-defined hyper-parameters.

Dual-branch Robust Unlearnable Examples

Table 1. Evaluation and comparison. The test accuracy (%) results on CIFAR-10 UE baselines across defenses with intra-architecture ResNet18 and cross-architecture VGG19 (since the surrogate model is ResNet18), where "AVG" indicates column-wise average values.

Model	Defense	EM	TAP	URP	LSP	AR	REM	SEP	OPS	CUDA	GUE	SEM	DH	DUNE
ResNet18	w/o	18.26±0.86	31.41±5.41	17.89±1.36	22.73±1.51	11.68±1.00	25.81±1.36	9.42±1.72	25.32±2.66	25.48±2.21	11.71±0.66	15.94±2.06	10.28±0.49	13.26±1.12
	AT	69.72±1.22	82.81±0.37	84.72±1.07	81.19±0.65	83.80±0.63	59.12±2.40	62.51±1.23	40.28±1.65	49.32±2.16	77.32±0.77	32.43±1.12	49.37±2.27	24.96±0.63
	AA	82.08±4.35	66.46±1.41	90.23±0.50	85.93±2.46	45.83±5.62	43.34±3.13	22.79±2.60	46.55±18.02	40.78±1.04	31.28±16.76	39.29±5.14	46.06±3.42	19.55±3.18
	OP	64.37±5.09	46.35±0.55	89.39±0.38	89.73±0.39	29.45±3.98	30.18±0.92	12.58±3.71	88.98±1.02	28.66±2.48	88.33±0.46	15.99±3.05	82.67±8.23	12.81±2.52
	ISS-G	89.09±0.60	20.99±1.43	60.94±6.96	67.83±7.38	38.87±1.92	66.16±5.55	9.66±1.84	27.33±2.43	22.89±3.23	89.52±0.31	31.94±0.81	14.03±4.04	10.18±1.53
	ISS-J	78.91±0.52	81.32±0.65	81.09±0.62	79.50±0.08	81.33±0.23	80.99±0.58	81.12±0.21	80.87±0.05	43.31±1.61	79.34±0.03	81.58±0.53	81.19±0.78	28.88±2.22
	ECLIPSE	82.07±0.86	86.33±0.20	87.08±0.54	84.58±0.32	87.16±0.24	82.05±1.03	82.59±0.51	61.47±0.36	34.18±1.79	85.60±0.77	85.82±0.49	87.22±0.36	57.49±2.17
	COIN	19.49±1.15	78.24±0.52	81.56±1.20	24.68±2.42	33.67±3.04	32.07±2.02	48.10±0.70	79.09±1.35	72.02±0.21	18.82±3.36	24.22±4.72	24.49±1.95	19.21±1.65
AVG	63.00±0.15	61.74±0.73	74.11±0.99	67.02±0.88	51.47±0.93	52.46±0.78	41.10±0.93	56.24±1.44	39.58±1.17	60.24±1.80	40.90±0.20	44.92±1.16	23.29±0.86	
VGG19	w/o	19.61±1.37	26.89±1.16	18.19±2.14	23.19±1.58	13.65±1.14	29.65±2.76	9.43±1.40	20.95±2.34	26.67±2.30	14.20±1.00	35.89±2.43	9.83±0.32	13.23±0.63
	AT	65.58±1.18	80.97±0.33	83.61±0.37	78.62±0.56	80.39±0.27	63.54±0.30	75.05±1.09	43.74±1.17	46.80±2.57	76.61±1.65	65.03±1.17	45.41±2.86	21.72±1.20
	AA	81.83±3.30	57.92±3.26	84.69±2.14	56.31±40.31	27.49±2.46	38.00±24.37	15.29±5.20	42.06±19.16	38.16±5.90	50.75±6.06	53.78±5.60	29.59±12.26	17.52±0.84
	OP	80.59±1.16	52.96±1.27	86.85±0.70	87.63±0.18	15.73±2.45	32.48±0.53	10.19±1.10	86.48±0.83	30.01±1.31	85.80±1.41	41.77±3.50	17.53±3.27	18.10±3.95
	ISS-G	86.40±0.53	26.18±1.47	62.44±2.22	81.74±0.95	37.76±2.03	70.96±1.04	7.26±3.11	19.24±2.13	19.52±3.40	88.16±0.68	44.67±0.93	10.35±0.17	10.00±1.32
	ISS-J	79.14±0.44	80.93±0.25	80.83±0.16	78.63±0.12	81.13±0.53	79.84±0.65	80.27±0.53	79.32±1.15	41.22±1.31	77.69±0.33	80.03±0.99	80.92±0.70	29.31±0.24
	ECLIPSE	78.78±1.69	84.59±0.36	85.27±0.73	83.85±0.33	85.21±1.18	80.47±0.50	80.59±0.47	64.64±1.61	32.37±0.32	83.63±0.80	80.27±8.43	85.67±0.49	56.38±1.26
	COIN	19.71±1.26	74.88±0.93	78.55±1.39	25.04±1.26	28.47±6.48	28.54±3.44	49.18±3.15	74.14±0.70	16.61±1.40	43.59±1.55	22.42±2.18	15.88±0.12	15.88±0.12
AVG	63.95±0.40	60.66±0.41	72.55±0.74	64.38±5.24	46.23±1.13	52.93±3.03	40.91±0.97	53.82±2.66	38.53±1.81	61.68±1.31	55.63±0.65	37.72±1.72	22.77±0.37	

Beyond the robustness gained from the dual-domain perturbations, this ensemble module provides an additional robustness boost (see Tab. 4), as analyzed below:

Remark II (*Loss landscape perspective*)

Ensemble-based optimization enhances robustness by reducing model-specific biases and smoothing the loss landscape (see Fig. 3). By averaging gradients across models, it preserves only cross-model shortcut directions, yielding more stable perturbations against diverse defense approaches.

Unlearnability-enhancing ensemble. To enhance the sample’s unlearnability, we leverage the idea of ensemble learning (Dong et al., 2020) into both of the spatial branch and color branch UE generation process, where combined models guide the optimization direction. Assuming there exists a checkpoint gallery composed of pre-trained models $\{f_{\theta_i}\}_{i=1}^M$, Eq. (9) is reformulated to derive g_t as below:

$$g_t = \frac{1}{M} \sum_{j=1}^M \nabla_{x_i} \mathcal{L}_{CE}(f_{\theta_j}(x_i^t), y_p^*) \quad (16)$$

Similarly, the cross-entropy loss \mathcal{L} in Eq. (14) is replaced by $\frac{1}{M} \sum_{j=1}^M \mathcal{L}_{CE}(f_{\theta_j}(x_i + \delta_{c_i}), y_p^*)$, which is a gradient-free ensemble loss term. These two formulations revert to vanilla ones when $M = 1$, implying that ensemble models are not utilized and only a single model is used. For class y_p , after obtaining $\{\delta_{s_i}\}_{i=1}^{n_p}$ and δ_c from the spatial and color branches, we generate the UE $x_{u_i} = x_i + \delta_{s_i} + \delta_c|_{i=1}^{n_p}$. Therefore, the unlearnable dataset \mathcal{D}_u is formulated as:

$$\mathcal{D}_u = \left\{ \underbrace{(x_{u_1}, y_p), (x_{u_2}, y_p), \dots, (x_{u_{n_p}}, y_p)}_{n_p \text{ unlearnable examples from class } y_p} \right\}_{p=1}^k \quad (17)$$

The framework of DUNE scheme is illustrated in Fig. 5, and the algorithm is described in Algorithm 1.

Table 2. The test accuracy on ImageNet UEs trained on ResNet18.

Defense ↓ UE →	EM	URP	LSP	REM	DUNE
w/o	2.80±0.17	55.28±2.42	19.39±1.18	20.93±3.13	6.78±0.31
AT (Tao et al., 2021)	44.02±0.53	44.05±1.18	43.33±2.17	31.65±1.97	15.00±0.41
AA (Qin et al., 2023)	53.40±2.50	53.27±2.74	49.80±2.30	51.64±1.10	49.22±2.49
ISS-G (Liu et al., 2023)	41.72±5.73	44.20±9.33	50.17±2.27	41.55±0.41	14.67±3.02
ISS-J (Liu et al., 2023)	41.12±3.69	56.53±1.16	52.35±3.26	24.23±2.11	7.93±0.99
COIN (Li et al., 2025)	3.12±0.24	50.28±2.43	34.80±4.57	19.02±1.31	6.40±0.49
AVG	31.03±1.08	50.60±0.63	41.64±0.99	31.50±1.35	16.67±0.30

5. Experiments

5.1. Experimental Details

Experimental setup. Following existing UE works (Li et al., 2025; Meng et al., 2024; Wang et al., 2024a), we employ CIFAR-10 (Krizhevsky & Hinton, 2009) and ImageNet (Deng et al., 2009) (select the first 100 classes) datasets, along with ResNet18 (He et al., 2016), VGG19 (Simonyan & Zisserman, 2014), DenseNet121 (Huang et al., 2017), EfficientNet-B0 (Tan & Le, 2019), and ViT (Khan et al., 2022; Shen et al., 2026) networks. We employ SGD for 80 epochs training with a momentum of 0.9, an initial learning rate of 0.1, and a batch size of 128 for CIFAR-10 and 256 for ImageNet. Regarding the DUNE implementation, f_{θ} is set to ResNet18, and the hyper-parameters M , β , T , N , λ , Δy , ϵ are empirically set to 5, 0.5, 30, 1000, 1.0, 3, 8/255, respectively. We select 7 SOTA defenses with their default implementations, including AT (Tao et al., 2021), AA (Qin et al., 2023), OP (Sandoval-Segura et al., 2023), ISS-G (Liu et al., 2023), ISS-J (Liu et al., 2023), ECLIPSE (Wang et al., 2024a), and COIN (Li et al., 2025), to evaluate the robustness of UEs.

Comparison baselines. We compare the robustness of our proposed UE scheme DUNE with 12 SOTA UE methods, covering EM (Huang et al., 2021), TAP (Fowl et al., 2021), URP (Tao et al., 2021), LSP (Yu et al., 2022), AR (Sandoval-

Algorithm 1 Our proposed DUNE scheme

Input: Clean $\mathcal{D}_c = \{(x_1, y_p), (x_2, y_p), \dots, (x_{n_p}, y_p)\}_{p=1}^k$; hyper-parameters $\beta, T, \epsilon, N, \lambda, \Delta y; \{f_{\theta_i}\}_{i=1}^M$.

Output: $\mathcal{D}_u = \{(x_{u_1}, y_p), (x_{u_2}, y_p), \dots, (x_{u_{n_p}}, y_p)\}_{p=1}^k$.

Initialize the checkpoints of $\{f_{\theta_i}\}_{i=1}^M$ with model training and dual-branch perturbations δ_s, δ_c ;

for $p = 1$ **to** k **do**

 /* Color-branch unlearnable generation */

 Initialize $\mathcal{L}_{color}=0$ and randomly select N image samples $\{x_i\}_{i=1}^N$ from class y_p ;

for $i = 1$ **to** N **do**

$\mathcal{L}_{color} += [\frac{1}{M} \sum_{j=1}^M \mathcal{L}_{CE}(f_{\theta_j}(x_i + \delta_c), y_p^*) + \lambda \mathcal{L}_{nc}]$;

end

 Search the optimal $\delta_c = \arg \min_{\text{PSO}} \mathcal{L}_{color}(\delta_c)$;

 /* Spatial-branch unlearnable generation */

for $i = 1$ **to** n_p **do**

for $t = 0$ **to** $T - 1$ **do**

 Ensemble $g_t = \frac{1}{M} \sum_{j=1}^M \nabla_{x_i^t} \mathcal{L}_{CE}(f_{\theta_j}(x_i^t), y_p^*)$;

$x_i^{t+1} = x_i^t - \beta \cdot \text{sign}(g_t)$;

$x_i^{t+1} = \min \left\{ \max \{ x_i^{t+1}, x_i^0 - \epsilon \}, x_i^0 + \epsilon \right\}$;

end

$x_{u_i} = x_i^T + \delta_c$; /* $x_i^T = x_i + \delta_{s_i}$ */

$x_{u_i} = \text{clamp}(x_{u_i}, 0, 1)$;

end

end

Return: $\mathcal{D}_u = \{(x_{u_1}, y_p), (x_{u_2}, y_p), \dots, (x_{u_{n_p}}, y_p)\}_{p=1}^k$.

Table 3. DUNE performance against ViT-based architectures.

Datasets Defenses	CIFAR-10		ImageNet-100	
	ViT-Tiny	ViT-Small	ViT-B/32	ViT-B/16
w/o	13.32±2.21	13.01±2.72	2.37±0.47	2.53±0.38
ISS-J	18.12±0.69	16.53±0.74	3.42±0.28	2.88±0.25
ISS-G	23.07±9.88	25.88±6.91	10.73±0.78	8.13±0.62

Segura et al., 2022), REM (Fu et al., 2022), SEP (Chen et al., 2023), OPS (Wu et al., 2023), CUDA (Sadasivan et al., 2023), GUE (Liu et al., 2024a), SEM (Liu et al., 2024b), and DH (Meng et al., 2024). These selected UEs cover perturbation forms based on convolution, ℓ_0 , ℓ_2 , and ℓ_∞ norms, enabling a systematic robustness assessment and comparison of existing baseline approaches.

Evaluation metrics. Consistent with previous UE literature (Meng et al., 2024; Li et al., 2025; Liu et al., 2024a; Huang et al., 2021), we evaluate UE performance by measuring the *test accuracy* (in %) of classifiers trained on unlearnable training datasets using clean test sets. Lower test accuracy indicates stronger unlearnability, while lower test accuracy under defense implies higher robustness of the UE. The test accuracy results of Tabs. 1 and 2 are reported as the average \pm standard deviation across three runs using diverse seeds.

Table 4. Ablation study on DUNE with CIFAR-10.

Model	Num.	SB	CB	UEE	w/o	AT	ISS-G	ISS-J	COIN	AVG
Res-Net18	①	✓			28.59	78.91	18.68	80.66	78.43	57.05
	②		✓		32.41	42.47	70.93	47.25	25.29	43.67
	③			✓	20.70	28.96	64.44	31.93	17.37	32.68
	④	✓		✓	12.77	77.50	9.82	80.65	70.26	50.20
	⑤	✓	✓		26.28	40.70	17.99	42.54	28.22	31.15
	⑥	✓	✓	✓	12.54	24.41	11.85	31.18	18.37	19.67
VGG-19	①	✓			30.56	62.96	16.56	80.40	77.81	53.66
	②		✓		29.67	33.61	79.28	40.37	25.46	41.68
	③			✓	18.28	22.06	57.60	29.05	16.91	28.78
	④	✓		✓	16.10	66.92	10.35	80.61	61.87	47.17
	⑤	✓	✓		23.75	30.41	20.49	39.75	21.15	27.11
	⑥	✓	✓	✓	13.67	20.59	10.89	29.30	15.98	18.09

5.2. Evaluation and Comparison

Effectiveness. As shown in Tab. 1, without applying defense, DUNE reduces the test accuracy of ResNet18 and VGG19 to 13.26% and 13.23%, respectively, which is comparable to random guessing on the test set. Meanwhile, on the ImageNet100 in Tab. 2, DUNE also underscores the test accuracy to 6.78%, further confirming the effectiveness of the proposed DUNE scheme in achieving unlearnability. The ViT results in Tab. 3 also reveal the robustness of DUNE.

Robustness. We evaluate the robustness of our proposed UE scheme DUNE under 7 diverse defense methods and further quantitatively compare its performance with 12 SOTA UE baselines, as demonstrated in Tabs. 1 and 2. Across diverse defenses, models, and datasets, DUNE consistently yields the lowest average test accuracy, reflecting the best overall robustness. Moreover, the highest accuracy achieved by applying 7 SOTA defenses to DUNE remains below 60%, significantly lower than that of clean trained models, *i.e.*, 80%~90%, indicating its superior robustness. As shown in Tab. 4, AT and ISS-J are primarily tailored to suppress high-frequency noise, and thus struggle against DUNE’s color-branch perturbations; conversely, ISS-G targets low-frequency noise but remains ineffective against spatial-branch perturbations. Consequently, our dual-branch design yields robustness against these defenses.

5.3. Ablation Study

To investigate the contribution of each component in DUNE, we conduct ablation studies, where the *spatial branch generation* module is denoted as SB, the *color branch generation* module as CB, and the *unlearnability-enhancing ensemble* module as UEE. As seen in Tab. 4, employing any single module or pair among SB, CB, and UEE yields lower average unlearnability performance across defenses compared with the DUNE scheme, confirming the critical contribution of each module. Meanwhile, it is observed that removing the UEE module (using only SB and CB), *i.e.*, optimizing perturbations with a single model, causes the unlearnability performance to decrease by 13.74% on ResNet18 and

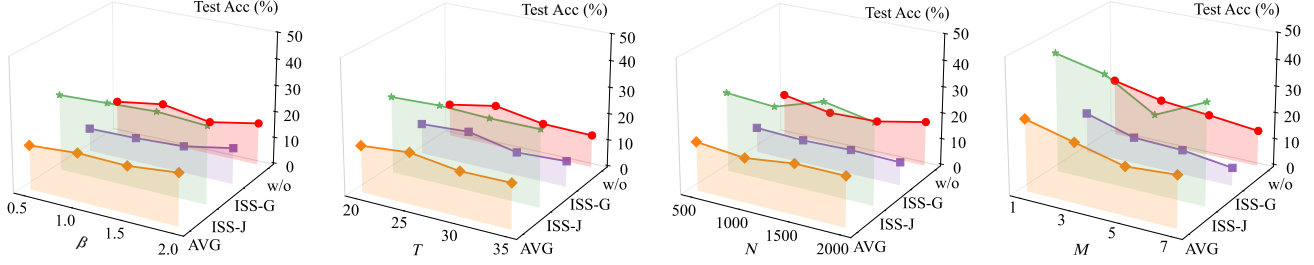


Figure 7. **Hyper-parameter sensitivity analysis.** The impact of hyperparameters β , T , N , and M on the test accuracy results (%) of the ResNet18 classifier trained on DUNE-generated CIFAR-10 dataset.

10.08% on VGG19, with robustness performance (under AT (Tao et al., 2021), ISS (Liu et al., 2023), COIN (Li et al., 2025)) also reduced by 5.17%-16.29%. These results indicate that UEE module plays a crucial role in improving the effectiveness and robustness of DUNE’s perturbations.

5.4. Hyper-parameter Analysis

We select four hyper-parameters, β , T , N , and M , each of which plays a critical role in different modules of DUNE. As shown in Fig. 7, the β and T of the spatial branch achieve the best average performance at 0.5 and 30, respectively. The overall trend remains stable, except that excessively large β degrades unlearnability. We attribute this to the overly large step hindering convergence in the spatial domain and weakening feature displacement. For the color branch parameter N , the best performance is achieved at $N = 1000$, where optimal unlearnability offsets in the color domain are obtained.

5.5. Resistance to Potential Adaptive Defenses

Formulation of adaptive defenses. Given that DUNE produces class-wise feature separation across the domains, we design an adaptive defense that introduces random noise in both domains to neutralize UEs, formulated as:

$$\forall x_u \sim \mathcal{D}_u, \quad x'_u \leftarrow x_u + \eta_c + \eta_s \quad (18)$$

where η_c denotes channel-wise random shifts, independently sampled for each RGB channel from $\mathcal{U}(-r_c, r_c)$, η_s represents spatial Gaussian noise sampled from $\mathcal{U}(0, r_s)$, and r_c and r_s respectively control the noise strength. We further consider an adaptive defense, which substitutes random Gaussian noise with adversarial noise through adversarial training, while η_c remains, formulated as:

$$\forall x_u \sim \mathcal{D}_u, \quad x'_u \leftarrow x_u + \eta_c, \quad (19)$$

$$\min_{\theta} \mathbb{E}_{(x'_u, y) \sim \mathcal{D}_u} \left[\max_{\|\eta_a\| \leq q_s} \mathcal{L}_{CE}(\mathcal{F}(x'_u + \eta_a; \theta), y) \right] \quad (20)$$

where $\eta_c \sim \mathcal{U}(-q_c, q_c)$, η_a is the adversarial noise during AT, and q_c and q_s control the strengths of the two noises.

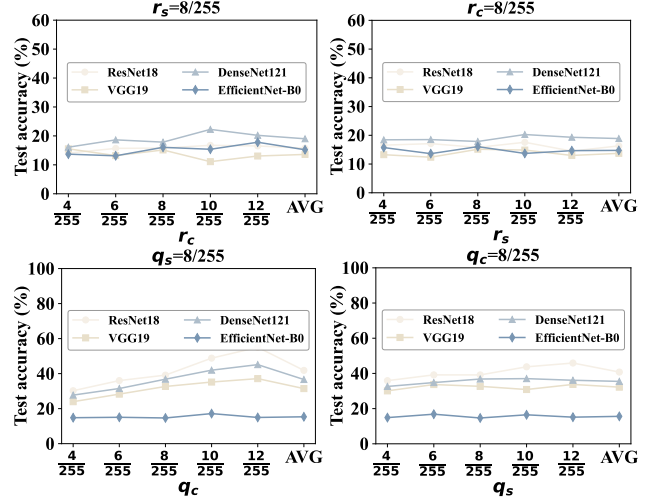


Figure 8. **Adaptive defenses.** DUNE performance under the two types of adaptive defenses on CIFAR-10.

Resistance of DUNE. The robustness of DUNE is evaluated under varying adaptive defense strengths across 4 model architectures, as demonstrated in Fig. 8. For the adaptive defense in Eq. (18), with either r_c or r_s held fixed, varying the random noise injected into another domain keeps the test accuracy of diverse models trained on DUNE data below 30%. For the adaptive defense in Eqs. (19) and (20), despite achieving better results than dual-branch random noise, the overall performance is relatively limited, further verifying the robustness of DUNE against such adaptive defenses.

6. Conclusion, Limitation, and Future Work

In this research, we propose DUNE, a dual-branch unlearnable example generation framework that jointly exploits spatial and color domain perturbations and enhances robustness through ensemble optimization. Unlike prior single-domain approaches, DUNE expands the unlearnable space while preserving semantic consistency, making it resistant to existing SOTA UE defenses. Extensive experiments on benchmark datasets demonstrate significant robustness improvements over existing UE methods. One current limitation is the focus on image classification tasks, future research will extend DUNE to multi-modal or real-world tasks.

Impact Statement

This work studies robust unlearnable examples that preserve human-perceived utility while making the data hard to learn from by unauthorized models. Robust UEs can offer meaningful privacy and intellectual-property protection for individuals and data owners (e.g., creators, institutions) by reducing the risk of non-consensual model training and downstream misuse. In settings where datasets are shared across parties, UEs may also provide a practical mechanism for enforcing data-governance policies without requiring changes to model architectures or training pipelines.

At the same time, the capability can be misused to deliberately degrade model training, disrupt public or community datasets, or interfere with legitimate research and safety efforts. Such misuse could amount to a denial-of-service vector against machine-learning development, especially in open-data ecosystems. To mitigate these risks, we encourage: (i) controlled distribution of protected data with clear licenses and consent, (ii) dataset integrity checks and provenance tracking, (iii) robust training-time detection and filtering mechanisms, and (iv) responsible disclosure and evaluation protocols. Overall, we believe robust UEs primarily advance user agency and data protection, while requiring careful governance to prevent adversarial abuse.

References

- Baack, S. A critical analysis of the largest source for generative ai training data: Common crawl. In *Proceedings of the ACM Conference on Fairness, Accountability, and Transparency*, pp. 2199–2208, 2024.
- Bakurov, I., Buzzelli, M., Schettini, R., Castelli, M., and Vanneschi, L. Structural similarity index (ssim) revisited: A data-driven approach. *Expert Systems with Applications*, 189:116087, 2022.
- Carlini, N., Jagielski, M., Choquette-Choo, C. A., Paleka, D., Pearce, W., Anderson, H., Terzis, A., Thomas, K., and Tramèr, F. Poisoning web-scale training datasets is practical. In *Proceedings of the 2024 IEEE Symposium on Security and Privacy (S&P'24)*, pp. 407–425. IEEE, 2024.
- Chen, S., Yuan, G., Cheng, X., Gong, Y., Qin, M., Wang, Y., and Huang, X. Self-ensemble protection: Training checkpoints are good data protectors. In *Proceedings of the 11th International Conference on Learning Representations (ICLR'23)*, 2023.
- Deng, J., Dong, W., Socher, R., Li, L.-J., Li, K., and Fei-Fei, L. Imagenet: A large-scale hierarchical image database. In *Proceedings of the 2009 IEEE/CVF Conference on Computer Vision and Pattern Recognition (CVPR'09)*, pp. 248–255, 2009.
- Dolatabadi, H. M., Erfani, S., and Leckie, C. The devil’s advocate: Shattering the illusion of unexploitable data using diffusion models. *arXiv preprint arXiv:2303.08500*, 2023.
- Dong, X., Yu, Z., Cao, W., Shi, Y., and Ma, Q. A survey on ensemble learning. *Frontiers of Computer Science*, 14(2):241–258, 2020.
- Fowl, L., Goldblum, M., Chiang, P.-y., Geiping, J., Czaja, W., and Goldstein, T. Adversarial examples make strong poisons. In *Proceedings of the 35th Conference on Neural Information Processing Systems (NeurIPS'21)*, volume 34, pp. 30339–30351, 2021.
- Fu, S., He, F., Liu, Y., Shen, L., and Tao, D. Robust unlearnable examples: Protecting data privacy against adversarial learning. In *Proceedings of the 10th International Conference on Learning Representations (ICLR'22)*, 2022.
- Geirhos, R., Jacobsen, J.-H., Michaelis, C., Zemel, R., Brendel, W., Bethge, M., and Wichmann, F. A. Shortcut learning in deep neural networks. *Nature Machine Intelligence*, 2:665–673, 2020.
- Guo, H., Niu, B., Huang, Y., Bai, X., Lan, F., and Zhao, P. Spread spectrum watermark in dc: A view from the embedding processing. *ACM Transactions on Multimedia Computing, Communications and Applications*, 2025.
- He, K., Zhang, X., Ren, S., and Sun, J. Deep residual learning for image recognition. In *Proceedings of the 2016 IEEE/CVF Conference on Computer Vision and Pattern Recognition (CVPR'16)*, pp. 770–778, 2016.
- Hu, S., Liu, W., Li, M., Zhang, Y., Liu, X., Wang, X., Zhang, L. Y., and Hou, J. Pointcrt: Detecting backdoor in 3d point cloud via corruption robustness. In *Proceedings of the 31st ACM International Conference on Multimedia (ACM MM'23)*, pp. 666–675, 2023.
- Huang, G., Liu, Z., Van Der Maaten, L., and Weinberger, K. Q. Densely connected convolutional networks. In *Proceedings of the 2017 IEEE/CVF Conference on Computer Vision and Pattern Recognition (CVPR'17)*, pp. 4700–4708, 2017.
- Huang, H., Ma, X., Erfani, S. M., Bailey, J., and Wang, Y. Unlearnable examples: Making personal data unexploitable. In *Proceedings of the 9th International Conference on Learning Representations (ICLR'21)*, 2021. URL <https://openreview.net/forum?id=iAmZUo0DxC0>.
- Jiang, W., Diao, Y., Wang, H., Sun, J., Wang, M., and Hong, R. Unlearnable examples give a false sense of security: Piercing through unexploitable data with learnable examples. In *Proceedings of the 31st ACM International Conference on Multimedia (MM'23)*, pp. 8910–8921, 2023.
- Kettunen, M., Härkönen, E., and Lehtinen, J. E-lpips: robust perceptual image similarity via random transformation ensembles. *arXiv preprint arXiv:1906.03973*, 2019.
- Khan, S., Naseer, M., Hayat, M., Zamir, S. W., Khan, F. S., and Shah, M. Transformers in vision: A survey. *ACM computing surveys*, 54(10s):1–41, 2022.
- Krizhevsky, A. and Hinton, G. Learning multiple layers of features from tiny images. 2009.
- Li, M., Wang, X., Yu, Z., Hu, S., Zhou, Z., Zhang, L., and Zhang, L. Y. Detecting and corrupting convolution-based unlearnable examples. In *Proceedings of the 39th AAAI Conference on Artificial Intelligence (AAAI'25)*, 2025.
- Liu, S., Wang, Y., and Gao, X.-S. Game-theoretic unlearnable example generator. In *Proceedings of the 38th AAAI Conference on Artificial Intelligence (AAAI'24)*, volume 38, pp. 21349–21358, 2024a.

- Liu, Y., Xu, K., Chen, X., and Sun, L. Stable unlearnable example: Enhancing the robustness of unlearnable examples via stable error-minimizing noise. In *Proceedings of the 38th AAAI Conference on Artificial Intelligence (AAAI'24)*, volume 38, pp. 3783–3791, 2024b.
- Liu, Z., Zhao, Z., and Larson, M. Image shortcut squeezing: Countering perturbative availability poisons with compression. In *Proceedings of the 40th International Conference on Machine Learning (ICML'23)*, 2023.
- Madry, A., Makelov, A., Schmidt, L., Tsipras, D., and Vladu, A. Towards deep learning models resistant to adversarial attacks. In *Proceedings of the 6th International Conference on Learning Representations (ICLR'18)*, 2018.
- Meng, R., Yi, C., Yu, Y., Yang, S., Shen, B., and Kot, A. C. Semantic deep hiding for robust unlearnable examples. *IEEE Transactions on Information Forensics and Security (TIFS'24)*, 2024.
- Pham, H., Ta, T.-A., Tran, A., and Doan, K. D. Flatness-aware sequential learning generates resilient backdoors. In *Proceedings of the European Conference on Computer Vision (ECCV'24)*, pp. 89–107. Springer, 2024.
- Qin, T., Gao, X., Zhao, J., Ye, K., and Xu, C.-Z. Learning the unlearnable: Adversarial augmentations suppress unlearnable example attacks. *arXiv preprint arXiv:2303.15127*, 2023.
- Sadasivan, V. S., Soltanolkotabi, M., and Feizi, S. Cuda: Convolution-based unlearnable datasets. In *Proceedings of the 2023 IEEE/CVF Conference on Computer Vision and Pattern Recognition (CVPR'23)*, pp. 3862–3871, 2023.
- Sandoval-Segura, P., Singla, V., Geiping, J., Goldblum, M., Goldstein, T., and Jacobs, D. W. Autoregressive perturbations for data poisoning. In *Proceedings of the 36th Conference on Neural Information Processing Systems (NeurIPS'22)*, volume 35, 2022.
- Sandoval-Segura, P., Singla, V., Geiping, J., Goldblum, M., and Goldstein, T. What can we learn from unlearnable datasets? In *Proceedings of the 37th Conference on Neural Information Processing Systems (NeurIPS'23)*, 2023.
- Shen, X., Cai, Y., Ning, R., Xin, C., and Wu, H. Df-logit: Data-free logic-gated backdoor attacks in vision transformers. *arXiv preprint arXiv:2602.03040*, 2026.
- Simonyan, K. and Zisserman, A. Very deep convolutional networks for large-scale image recognition. *arXiv preprint arXiv:1409.1556*, 2014.
- Sun, Y., Zhang, H., Zhang, T., Ma, X., and Jiang, Y.-G. Unseg: One universal unlearnable example generator is enough against all image segmentation. In *Proceedings of the Conference on Neural Information Processing Systems (NeurIPS'24)*, volume 37, pp. 79168–79193, 2024.
- Tan, M. and Le, Q. Efficientnet: Rethinking model scaling for convolutional neural networks. In *Proceedings of the International Conference on Machine Learning (ICML'19)*, pp. 6105–6114. PMLR, 2019.
- Tanchenko, A. Visual-psnr measure of image quality. *Journal of Visual Communication and Image Representation*, 25(5): 874–878, 2014.
- Tao, L., Feng, L., Yi, J., Huang, S.-J., and Chen, S. Better safe than sorry: Preventing delusive adversaries with adversarial training. In *Proceedings of the 35th Conference on Neural Information Processing Systems (NeurIPS'21)*, volume 34, pp. 16209–16225, 2021.
- Wang, D., Tan, D., and Liu, L. Particle swarm optimization algorithm: an overview. *Soft Computing*, 22(2):387–408, 2018.
- Wang, R., Huang, Z., Chen, Z., Liu, L., Chen, J., and Wang, L. Anti-forgery: Towards a stealthy and robust deepfake disruption attack via adversarial perceptual-aware perturbations. In *Proceedings of the 31st International Joint Conference on Artificial Intelligence (IJCAI'22)*, 2022.
- Wang, X., Hu, S., Zhang, Y., Zhou, Z., Zhang, L. Y., Xu, P., Wan, W., and Jin, H. Eclipse: Expunging clean-label indiscriminate poisons via sparse diffusion purification. In *Proceedings of the 29th European Symposium on Research in Computer Security (ESORICS'24)*, 2024a.
- Wang, X., Li, M., Liu, W., Zhang, H., Hu, S., Zhang, Y., Zhou, Z., and Jin, H. Unlearnable 3D point clouds: Class-wise transformation is all you need. In *Proceedings of the 38th Neural Information Processing Systems (NeurIPS'24)*, volume 37, pp. 99404–99432, 2024b.
- Wang, X., Li, M., Xu, P., Liu, W., Zhang, L. Y., Hu, S., and Zhang, Y. Pointapa: Towards availability poisoning attacks in 3d point clouds. In *Proceedings of the European Symposium on Research in Computer Security (ESORICS'24)*, pp. 125–145. Springer, 2024c.
- Wang, X., Pan, H., Zhang, H., Li, M., Hu, S., Zhou, Z., Xue, L., Liu, A., Jiang, Y., Zhang, L. Y., et al. Trojanrobot: Physical-world backdoor attacks against vlm-based robotic manipulation. *arXiv preprint arXiv:2411.11683*, 2024d.
- Wang, X., Pan, W., Zhou, S., Li, K., Wang, Y., Ye, Z., Zhang, H., Zhang, L. Y., and Jia, X. Image-to-video diffusion: From foundations to open frontiers. 2026.
- Wu, Q., Yu, Y., Kong, C., Liu, Z., Wan, J., Li, H., Kot, A. C., and Chan, A. B. Temporal unlearnable examples: Preventing personal video data from unauthorized exploitation by object tracking. In *Proceedings of the IEEE/CVF International Conference on Computer Vision (ICCV'25)*, pp. 11110–11121, 2025.
- Wu, S., Chen, S., Xie, C., and Huang, X. One-pixel shortcut: on the learning preference of deep neural networks. In *Proceedings of the 11th International Conference on Learning Representations (ICLR'23)*, 2023.
- Yu, D., Zhang, H., Chen, W., Yin, J., and Liu, T.-Y. Availability attacks create shortcuts. In *Proceedings of the 28th ACM SIGKDD Conference on Knowledge Discovery and Data Mining (KDD'22)*, pp. 2367–2376, 2022.
- Yu, Y., Wang, Y., Xia, S., Yang, W., Lu, S., Tan, Y.-P., and Kot, A. C. Purify unlearnable examples via rate-constrained variational autoencoders. *arXiv preprint arXiv:2405.01460*, 2024a.
- Yu, Y., Zheng, Q., Yang, S., Yang, W., Liu, J., Lu, S., Tan, Y.-P., Lam, K.-Y., and Kot, A. Unlearnable examples detection via iterative filtering. In *Proceedings of the International Conference on Artificial Neural Networks (ICANN'24)*, pp. 241–256. Springer, 2024b.

Yu, Y., Xia, S., Yang, S., Kong, C., Yang, W., Lu, S., Tan, Y.-P., and Kot, A. C. Mtl-ue: Learning to learn nothing for multi-task learning. In *Proceedings of the 42nd International Conference on Machine Learning (ICML'25)*, 2025.

Zhang, H., Hu, S., Wang, Y., Zhang, L. Y., Zhou, Z., Wang, X., Zhang, Y., and Chen, C. Detector collapse: Backdooring object detection to catastrophic overload or blindness. *arXiv preprint arXiv:2404.11357*, 2024.

Zhao, Z., Liu, Z., and Larson, M. Adversarial image color transformations in explicit color filter space. *IEEE Transactions on Information Forensics and Security (TIFS'23)*, 18:3185–3197, 2023.

Zhu, Y., Yu, L., and Gao, X.-S. Detection and defense of unlearnable examples. In *Proceedings of the 38th AAAI Conference on Artificial Intelligence (AAAI'24)*, volume 38, pp. 17211–17219, 2024.